Saturation of the Inverse Cascade in Surface Gravity-Wave Turbulence

E. Falcon,[1,*] G. Michel,[2] G. Prabhudesai,[3] A. Cazaubiel,[1] M. Berhanu,[1]
N. Mordant,[4] S. Aumaître,[5] and F. Bonnefoy[6]
[1]*Université de Paris, Univ Paris Diderot, MSC, UMR 7057 CNRS, F-75 013 Paris, France*
[2]*Sorbonne Université, IJLRA, UMR 7190 CNRS, F-75 005 Paris, France*
[3]*Ecole Normale Supérieure, LPS, UMR 8550 CNRS, F-75 205 Paris, France*
[4]*Université Grenoble Alpes, LEGI, UMR 5519 CNRS, F-38 000 Grenoble, France*
[5]*CEA-Saclay, Sphynx, DSM, URA 2464 CNRS, F-91 191 Gif-sur-Yvette, France*
[6]*Ecole Centrale de Nantes, LHEEA, UMR 6598 CNRS, F-44 321 Nantes, France*

(Received 4 May 2020; accepted 14 August 2020; published 21 September 2020)

We report on the observation of surface gravity-wave turbulence at scales larger than the forcing ones in a large basin. In addition to the downscale transfer usually reported in gravity-wave turbulence, an upscale transfer is observed, interpreted as the inverse cascade of weak turbulence theory. A steady state is achieved when the inverse cascade reaches a scale in between the forcing wavelength and the basin size, but far from the latter. This inverse cascade saturation, which depends on the wave steepness, is probably due to the emergence of nonlinear dissipative structures such as sharp-crested waves.

DOI: 10.1103/PhysRevLett.125.134501

Introduction.—Wave turbulence is a phenomenon exhibited by random nonlinear waves in interaction. It occurs in various contexts: ocean surface waves, plasma waves, hydroelastic or elastic waves, internal waves, or optical waves [1–4]. Nonlinear wave interactions are the basic mechanism that transfers the energy from a large (forcing) scale down to a small (dissipative) scale. Most experiments on wave turbulence concern its small-scale properties resulting from this direct energy cascade [5,6], notably to compare them with weak turbulence theory (WTT) [2,3]. The large-scale properties (i.e., larger than the forcing scale) have been much less investigated experimentally [7–10], although their understanding is of primary interest (e.g., for climate modeling and long-term weather forecasting). For instance, for systems involving four-wave interactions such as deep water gravity waves, an inverse cascade from the forcing scales towards a larger (dissipative) scale was predicted in the 1980s by WTT, due to an additional conserved quantity (wave action) [11]. It was confirmed by direct numerical simulations of Zakharov equations more than ten years ago [12,13]. To our knowledge, the only laboratory observation of inverse cascade in gravity-wave turbulence is limited to a narrow inertial range due to the small-sized container used [7], while recent attempts have been inconclusive within a larger size basin [14] or using another type of forcing [15]. As for field observations, inverse cascade is hardly distinguishable from the direct cascade due to the anisotropy, inhomogeneity, and nonstationnarity of the wind-generated wave fields [15–17]. A downshifting of the spectrum peak is rather reported as the wind strength or fetch grows [17–19].

In this Letter, we report the first laboratory experiment in a large-scale basin evidencing the formation of an inverse cascade of gravity waves. To do this, it has been found necessary to replace the usual absorbing beach of large basins by a reflective wall, and to use a multidirectional forcing to foster wave interactions. The cascade is found to stop well before a so-called condensate state is reached; i.e., before wave action piles up at a large scale due to basin finite size effects. Instead, a saturation is observed resulting from the emergence of highly dissipative nonlinear structures. Although well understood in 2D hydrodynamic turbulence [20] or Bose-Einstein condensation [21,22], such large-scale dynamics resulting from an inverse cascade is far from being fully understood for wave turbulence systems beyond gravity surface waves [7], such as for optical waves [8], waves in superfluid [9], plasma waves [23], or elastic waves [24,25].

Theoretical background.—The dispersion relation of linear deep-water surface gravity waves is $\omega(k) = \sqrt{gk}$, with $\omega = 2\pi f$ as the angular frequency, k as the wave number, and g as the acceleration of gravity. For weakly nonlinear interacting waves in a stationary out-of-equilibrium state within an infinite size system, WTT predicts the spectrum of surface elevation S_η for scales larger than the forcing one (inverse cascade) for a wave action flux Q (per unit surface and density) [11]

$$S_\eta^i(f) \sim Q^{1/3} g f^{-11/3}, \tag{1}$$

or for an energy flux P cascading from large to small scales (direct cascade) $S_\eta^d(f) \sim P^{1/3} g f^{-4}$ [26]. $S_\eta(f)$ has dimension L^2T, P has dimension $(L/T)^3$, and $[Q] = [P]/[\omega]$.

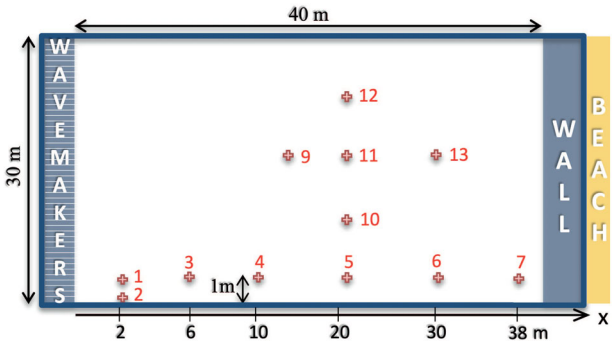

FIG. 1. Experimental setup showing the 48 flaps wave maker, the ending wall, and the locations of the 12 wave probes.

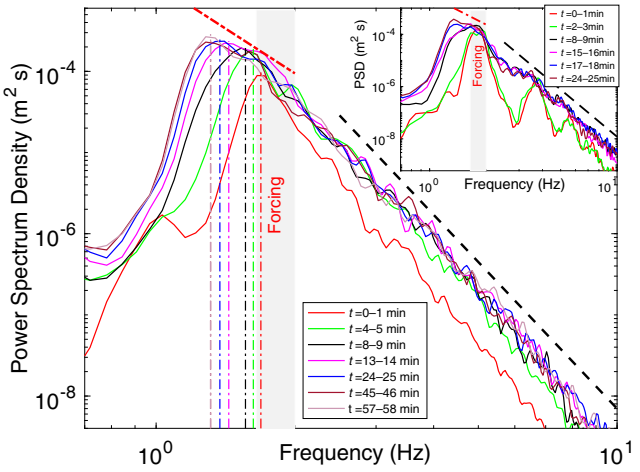

FIG. 2. Temporal evolution of the power spectrum density (PSD) of the wave height at $x = 20$ m (averaged on four probes n°5, 10, 11, 12—see Fig. 1). $\sigma_\eta = 1.14$ cm. Gray area: forcing bandwidth. Dash-dotted vertical lines correspond to the maximum of each spectrum. Dash-dotted red line is the prediction in $f^{-11/3}$ of Eq. (1). Dashed black line displays a f^{-6} fit. Inset: same for $x = 2$ m (averaged on probes n°1, 2).

WTT assumes a timescale separation between the nonlinear time, which reads for the inverse cascade $\tau_{\rm nl}^i \sim Q^{-2/3} g^{1/6} k^{-11/6}$, and the linear timescale $\tau_{\rm lin} = 1/\omega$, that is the nonlinearity parameter $\tau_{\rm lin}/\tau_{\rm nl}^i \sim Q^{2/3} g^{-2/3} k^{4/3} \ll 1$ [4]. As nonlinearity increases with Q, breaking of weak turbulence is expected to occur for $Q > Q_c = g/k^2$.

Experimental setup.—Experiments were performed in the large-scale wave basin (40 m long × 30 m wide × 5 m deep) at Ecole Centrale de Nantes with a wave maker made of 48 independently controlled flaps located at one end of the basin (see Fig. 1). To favor homogeneity, wave reflections, and wave interactions necessary to observe an inverse cascade, a solid wall is built at the opposite end instead of the usual absorbing sloping beach. A multidirectional random wave forcing is generated around a central frequency $f_0 = 1.8$ Hz within a narrow spectral bandwidth $f_0 \pm \Delta f$ with $\Delta f = 0.2$ Hz. To be able to observe waves at lower frequencies than the forcing ones, f_0 is chosen to be close to the high-frequency limit of the wave maker. The 2D multidirectional forcing is also crucial to ensure a spatially homogeneous wave field, and to avoid the direct excitation of the first basin eigenmodes (∼0.1–0.3 Hz). The surface elevation $\eta(t)$ is recorded during one hour by means of an array of 12 resistive wave probes located at different distances x from the wave maker ($x = 2$ to 38 m—see Fig. 1). Their vertical resolution is approximately 0.1 mm, their frequency resolution close to 20 Hz, and the sampling frequency 128 Hz. The typical rms wave height $\sigma_\eta \equiv \sqrt{\langle \eta^2(t) \rangle_t}$ is less than 2 cm, and the wave steepness $\epsilon \lesssim 0.1$ to limit to a weakly nonlinear wave regime. The central wavelength generated is $\lambda_0 = g/(2\pi f_0^2) \simeq 0.48$ m. The basin length is thus $83\lambda_0$ (assuming an unrealistic 1D monochromatic propagation), and a round-trip from the wave maker lasts $T \simeq 3$ min [group velocity $\omega_0/(2k_0) \simeq 0.44$ m/s].

Wave spectrum.—The temporal evolution of the power spectrum of the surface elevation recorded close to the wave maker ($x = 2$ m) is shown in the inset of Fig. 2, the spectrum being computed over 1 min intervals. For $t \lesssim T$, the wave spectrum displays peaks at the forcing frequencies and at their harmonics, as expected. After typically more than a wave round trip ($t > T$), the main spectrum peak undergoes a shift towards low frequencies (or large scales), whereas frequency power laws are observed at both low and high frequencies compared to the forcing ones. These two observations are related to the wave interaction dynamics occurring cumulatively after a while, and is not a wave maker's signature. Note that the direct cascade towards high frequency differs significantly from WTT prediction in f^{-4}, as reported earlier in different basin sizes [27–29], this departure being ascribed to the modulation of bound waves [30,31]. Numerical simulations have also evidenced departures from this prediction resulting from the occurrence of an inverse cascade [13]. Concerning the large-scale transfer, the frequency downshifting of the main peak is observed homogeneously within the basin (see below). For instance, in the middle of the basin (see main Fig. 2), the spectral peak $f_{\rm max}$ is shifted with time towards low frequencies and the spectral shape is compatible with the inverse cascade prediction of WTT in $f^{-11/3}$ of Eq. (1) (see dash-dotted red line). Although this experimental downshifting occurs in a narrow range (1/6 decade width in f) it corresponds to 1/3 decade in k, a result similar to the ones achieved in numerical simulations of this inverse cascade [12,13]. The saturation of this inverse cascade is also of interest: the wave spectrum reaches a stationary state in which the gravest eigenmodes are not excited and no condensate is observed. Since viscous dissipation is weak at these large scales (see below), it means that additional dissipation occurs to stop the inverse cascade.

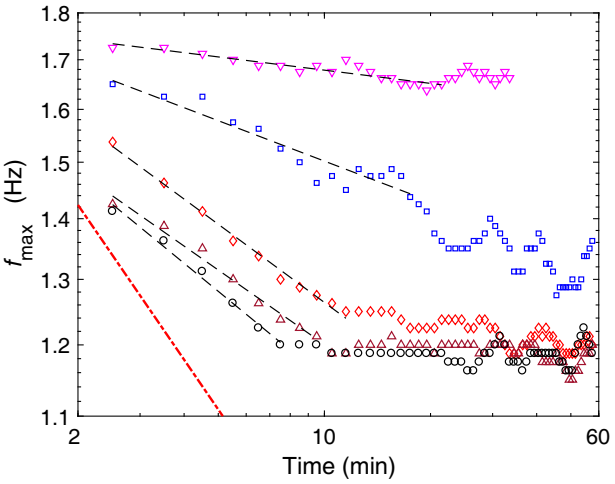

FIG. 3. Frequency of the spectrum maximum, f_{max}, over time for different forcing amplitudes. $\sigma_\eta^{sat} = (\nabla)$ 0.59, (square) 1.19, (diamond) 1.54, (triangle) 1.83, and (circle) 1.92 cm. Dash-dotted line is the prediction $t^{-3/11}$ [32]. Dashed lines are best power-law fits, at short times. $x = 20$ m.

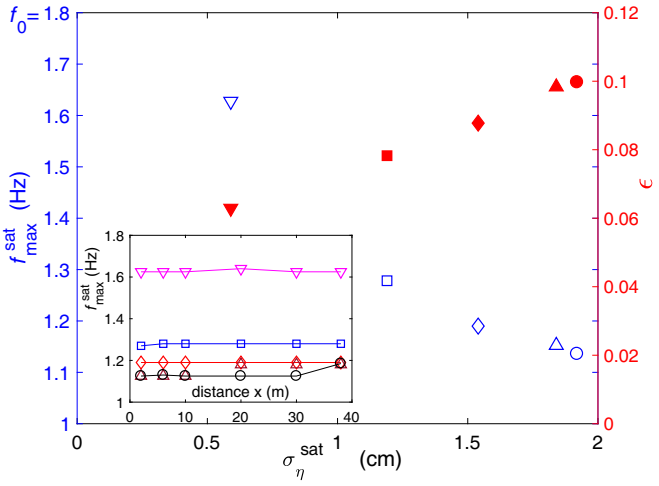

FIG. 4. Left-hand axis: saturation frequency f_{max}^{sat} reached by the spectrum versus forcing amplitude at $x = 20$ m (blue open symbols). Right-hand axis: wave steepness ϵ versus forcing at $x = 20$ m (red full symbols). Inset: f_{max}^{sat} for different distances x along the basin and different forcing amplitudes. Same symbols as inset of Fig. 3.

Saturation.—To better quantify this saturation, we report in Fig. 3 the frequency of the spectrum maximum, f_{max}, versus time along with the WTT prediction $f_{max} \sim t^{-3/11}$ which assumes a linear growth of the total wave action $N \sim t^1$ [32,33] (see dash-dotted red line). At short times, experimental values of f_{max} are found to be of the form $t^{-\alpha}$ but $\alpha \in [0.1, 0.15]$ differs from the theoretical exponent $(-3/11 = -0.273)$. This departure could be ascribed to small scale dissipation not being negligible during this transient regime as well as the presence of a dual cascade, contrary to the assumption of WTT. Because of the interaction between the wave maker and the wave field, a constant wave action flux may also not be achieved (i.e., $N \sim \int Q dt \sim t^1$). Indeed, following [32,33], one finds that the total wave action growth should scale as $N \sim t^{(11\alpha-1)/2}$ that is between $t^{0.05}$ and $t^{0.35}$ using our values of α. For long enough times, we observe that f_{max} saturates, and all the faster as the forcing amplitude increases (see Fig. 3—long time oscillations of the spectral peak are related to spectrum resolution $\simeq 0.06$ Hz). This saturation frequency f_{max}^{sat} decreases as the forcing amplitude increases (see main Fig. 4), and is independent of the measurement location within the basin (see inset of Fig. 4), confirming the homogeneity of the wave field observed directly from the shore.

To confirm that the inverse cascade dictates the saturation timescale of this system, we consider the temporal evolution of the standard deviation of the wave height $\sigma_\eta(t) = \sqrt{\int S_\eta(\omega, t) d\omega}$, again in the middle of the basin (see Fig. 5). A logarithmic growth $\sigma_\eta(t) = \gamma \log(t/t_0) + \sigma_\eta^{t_0}$ is clearly observed followed by a saturation to a value σ_η^{sat} occurring at t_{sat}. The saturation time $t_{sat} = t_0 \exp[(\sigma_\eta^{sat} - \sigma_\eta^{t_0})/\gamma]$ is found to be about 10–20 min ($\gamma \in [0.1, 0.4]$ cm and $t_0 = 1$ min), and to be consistent with the one related to f_{sat} as displayed in Fig. 5. This demonstrates that, as could be inferred from the spectra reported in Fig. 2, a statistically steady state is reached when the *inverse* cascade saturates. Both estimates show that the saturation times are much more than a typical wave packet round-trip (3 min assuming 1D propagation), and

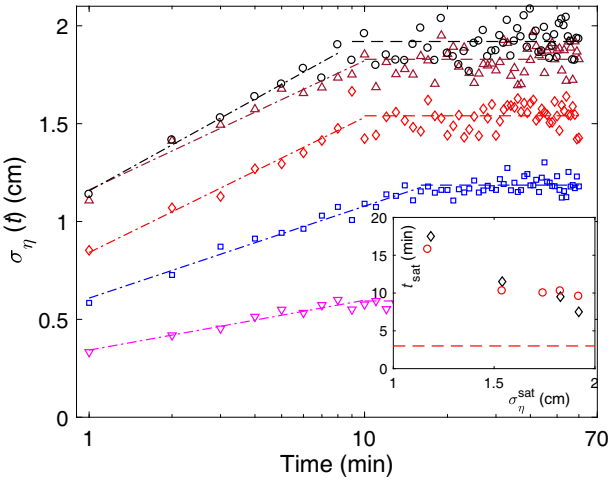

FIG. 5. Logarithmic time evolution of $\sigma_\eta(t)$ for different forcing amplitudes (same symbols as Fig. 3). Dash-dotted lines show logarithmic growth fits. Dashed lines shows the saturation values σ_η^{sat}. Inset: saturation times of (circle) $\sigma_\eta(t)$ and of (diamond) the spectrum evolution (inferred from Fig. 3) versus forcing. Dashed line corresponds to the typical wave packet round-trip (3 min). $x = 20$ m.

decrease with the forcing amplitude, or with the wave steepness $\epsilon \equiv k_{\max}\sigma_\eta^{\rm sat} = (2\pi f_{\max}^{\rm sat})^2\sigma_\eta^{\rm sat}/g$, the right-hand axis of Fig. 4 showing the relationship $\epsilon(\sigma_\eta^{\rm sat})$.

So, what stops the inverse cascade? Since energy (and wave action) is continuously injected into this closed system, a steady state must involve either linear dissipation or nonlinear localized dissipative structures (e.g., sharp-crested waves, whitecapping [13], wave breakings, bound waves [30,31,34], or parasitic gravity-capillary waves [35]). Prevailing linear dissipation at a wave frequency f_0 occurs in the viscous surface and basin lateral boundary layers yielding a typical decay time of $\tau_{\rm diss} > 3000$ s [36]. This timescale is such that the scale separation required by WTT is verified, $\tau_{\rm lin}(f) \ll \tau_{\rm nl}^i(f) \ll \tau_{\rm diss}(f)$, between the linear propagation time $\tau_{\rm lin} = 1/\omega$, the nonlinear interaction time $\tau_{\rm nl}^i$ and the dissipative time $\tau_{\rm diss}$, for our range of f. Indeed, using the values of Q and P inferred experimentally (see below), and using the dimensionless constant value found experimentally for $\tau_{\rm nl}$ [28], one finds $\tau_{\rm nl}^i$ at least two decades shorter (longer) than $\tau_{\rm diss}$ ($\tau_{\rm lin}$), with no fitting parameter (see the Supplemental Material [37]). The typical discreteness $\tau_{\rm disc}$ (i.e., inverse of the frequency separation of adjacent eigenmodes) is also found to be almost two decades longer than $\tau_{\rm nl}^i$ at the saturation frequency (see the Supplemental Material [37]). Basin finite size effects are thus unlikely to affect the dynamics (see case n°1 in [38]). The saturation time (shorter than $\tau_{\rm diss}$ and $\tau_{\rm disc}$) depends on the wave steepness. It is thus due to a nonlinear effect, probably related to the sharp-crested waves, occurring homogeneously in the wave field, and visible directly from the shore once a steady state is reached (see movies in [37]). Dissipation by nonlinear localized structures in the energy balance equation is indeed often referred in forecasting models of wind-driven ocean waves [32,39] and remains very challenging to estimate. Numerical simulations of fully nonlinear equations demonstrate that such structures are enhanced in the presence of an inverse cascade [13], and induce an effective large-scale dissipation not taken into account in WTT [40,41]. However, we have currently no way to quantify it since the wave probes are distributed discreetly over the basin surface, and localized structures are most of the time not captured. Indeed, the probability distributions of $\eta(t)$ and of $\partial\eta(t)/\partial t$ are found similar before and after the saturation, and close to a Tayfun distribution. Spatiotemporal measurements seem necessary to ascertain the role of localized structures, for instance by measuring the nonlinear corrections to the dispersion relation (see [42] for a numerical study), but are difficult to implement in such a large wave basin [29].

Wave action flux.—One can finally estimate the mean cascading wave action flux Q from the wave energy decay, notably to check further theoretical predictions of WTT. After 60 min of stationary wave turbulence, the wave maker is suddenly stopped at time $t = 0$, and the temporal decay

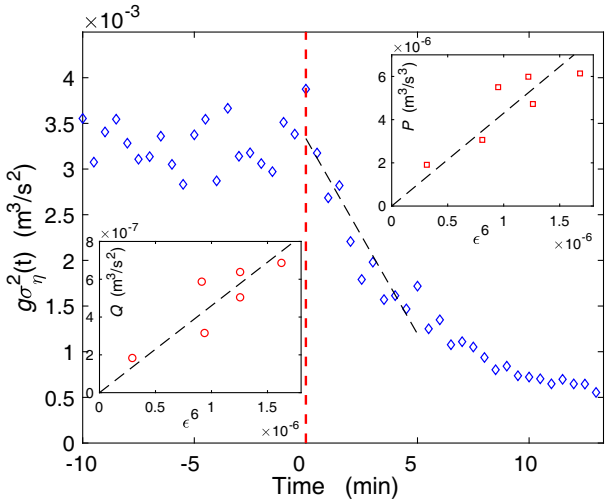

FIG. 6. Temporal evolution of the gravity wave energy. Wave maker is stopped at $t = 0$. Dashed line: tangent at $t = 0$ of slope $P = 5.98 \times 10^{-6}$ m^3/s^3. $\sigma_\eta^{\rm sat} = 1.82$ cm. $x = 20$ m. Mean energy flux P (top inset) and mean wave action flux Q (bottom inset) versus wave steepness to the power 6 from decaying experiments (main).

of the wave height is recorded during up to 30 min. Using the expressions of the gravity wave energy $E(t) = g\sigma_\eta^2(t)$ and of the power budget, the mean energy flux P (per unit surface and density) is given by $P = -gd\sigma_\eta^2(t)/dt|_{t=0}$ [28]. P is thus experimentally estimated from the tangent at $t = 0$ (see main Fig. 6), and the wave action flux from $Q \sim P/\omega_0$. We observe that Q (and P) increases linearly with ϵ^6 as expected theoretically [12,43]. Beyond this agreement with WTT, Q is found to be at least four orders of magnitude smaller than the critical flux breaking weak turbulence, $Q_c = g^2/\omega_0^4 \simeq 6 \times 10^{-3}$ m^3 s^{-2}, regardless ϵ.

Conclusion.—We reported the formation of an inverse cascade of gravity-wave turbulence in a large-scale closed basin. Although it satisfies some assumptions of WTT [weak nonlinearity, timescale separation, scaling of $Q(\epsilon)$, and homogeneity], its time evolution is found to be stopped well before wavelengths sizable to the length of the basin are observed. This contrasts with the only laboratory observation performed so far in a small-scale basin where finite size-effects stops the inverse cascade [7]. Here, the saturation is related to a nonlinear effect probably the occurrence of highly dissipative nonlinear structures (sharp-crested waves) visible in the wave field. Our findings could be useful in different wave turbulence fields involving an inverse cascade such as Langmuir waves in plasmas [23], Kelvin waves in quantum fluids [9], or for elastic waves in thin plates where coherent structures were shown numerically to limit the inverse cascade dynamics [24]. More generally, better identifying the mechanisms (such as inverse cascade) governing large-scale properties of turbulent flows is of paramount interest [44].

We thank S. Lambert, B. Pettinoti, and J. Weis (ECN) for their technical help on the experimental setup. Part of this work was supported by the French National Research Agency (ANR DYSTURB Project No. ANR-17-CE30-0004), and by a grant from the Simons Foundation MPS No. 651463-Wave Turbulence. N. M. is supported by European Research Council (Grant No. ERC No. 647018-WATU).

*eric.falcon@univ-paris-diderot.fr

[1] E. Falcon, Discrete Contin. Dyn. Syst. B **13**, 819 (2010).
[2] V. E. Zakharov, V. S. L'vov, and G. Falkovich, *Kolmogorov Spectra of Turbulence I: Wave Turbulence* (Springer, Berlin, 1992).
[3] S. Nazarenko, *Wave Turbulence* (Springer, Berlin, 2011).
[4] A. C. Newell and B. Rumpf, Annu. Rev. Fluid Mech. **43**, 59 (2011).
[5] *Advances in Wave Turbulence*, edited by V. Shrira and S. Nazarenko, Vol. 83 (World Scientific, Singapore, 2013).
[6] E. Falcon, Wave turbulence: A Set of stochastic nonlinear waves in interaction, in *Proceedings of the 5th ICAND 2018*, edited by V. In, P. Longhini and A. Palacios (Springer Nature, New York, 2019), Chap. 25, p. 259–266.
[7] L. Deike, C. Laroche, and E. Falcon, Europhys. Lett. **96**, 34004 (2011).
[8] U. Bortolozzo, J. Laurie, S. Nazarenko, and S. Residori, J. Opt. Soc. Am. B **26**, 2280 (2009); J. Laurie, U. Bortolozzo, S. Nazarenko, and S. Residori, Phys. Rep. **514**, 121 (2012).
[9] A. N. Ganshin, V. B. Efimov, G. V. Kolmakov, L. P. Mezhov-Deglin, and P. V. E. McClintock, Phys. Rev. Lett. **101**, 065303 (2008).
[10] G. Michel, F. Pétrélis, and S. Fauve, Phys. Rev. Lett. **118**, 144502 (2017).
[11] V. E. Zakharov and M. M. Zaslavskii, Izv. Acad. Sci., USSR, Atmos. Oceanic Phys. (Engl. Transl.) **18**, 747 (1982); Note that this prediction was published first in V. E. Zakharov, Some aspects of nonlinear theory of surface waves, Ph.D. thesis, Institute for Nuclear Physics, Novosibirsk, Russia, 1966 (in Russian).
[12] S. Y. Annenkov and V. I. Shrira, Phys. Rev. Lett. **96**, 204501 (2006).
[13] A. O. Korotkevich, Phys. Rev. Lett. **101**, 074504 (2008); Math. Comput. Simul. **82**, 1228 (2012).
[14] A. Campagne, R. Hassaini, I. Redor, J. Sommeria, and N. Mordant, in *Turbulent Cascades II*, edited by M. Gorokhovski and F. S. Godeferd (Springer International Publication, Cham, 2019), pp. 239–246.
[15] S. Nazarenko and S. Lukaschuk, Annu. Rev. Condens. Matter Phys. **7**, 61 (2016).
[16] M. A. Donelan, J. Hamilton, and W. H. Hui, Phil. Trans. R. Soc. A **315**, 509 (1985); P. A. Hwang, D. W. Wang, E. J. Walsh, W. B. Krabill, and R. N. Swift, J. Phys. Oceanogr. **30**, 2753 (2000); C. E. Long and D. T. Resio, J. Geophys. Res. **112**, C05001 (2007); F. Leckler, F. Ardhuin, C. Peureux, A. Benetazzo, F. Bergamasco, and V. Dulov, J. Phys. Oceanogr. **45**, 2484 (2015).
[17] L. Romero and W. K. Melville, J. Phys. Oceanogr. **40**, 441 (2010).
[18] S. Kawai, J. Fluid Mech. **93**, 661 (1979).
[19] T. Hara and C. C. Mei, J. Fluid Mech. **230**, 429 (1991).
[20] R. H. Kraichnan, Phys. Fluids **10**, 1417 (1967); J. Sommeria, J. Fluid Mech. **170**, 139 (1986); J. Paret and P. Tabeling, Phys. Rev. Lett. **79**, 4162 (1997).
[21] C. Connaughton, C. Josserand, A. Picozzi, Y. Pomeau, and S. Rica, Phys. Rev. Lett. **95**, 263901 (2005).
[22] C. Sun, S. Jia, C. Barsi, S. Rica, A. Picozzi, and J. W. Fleischer, Nat. Phys. **8**, 470 (2012).
[23] A. B. Kats and V. M. Kontorovich, JETP Lett. **14**, 265 (1971), http://www.jetpletters.ac.ru/ps/1629/article_24915.shtml; Y.-Y. Tsai, M.-C. Chang, and Lin I, Phys. Rev. E **86**, 045402(R) (2012).
[24] G. Düring, C. Josserand, and S. Rica, Phys. Rev. E **91**, 052916 (2015).
[25] R. Hassaini, N. Mordant, B. Miquel, G. Krstulovic, and G. Düring, Phys. Rev. E **99**, 033002 (2019).
[26] V. E. Zakharov and N. N. Filonenko, Sov. Phys. Dokl. **11**, 881 (1967).
[27] E. Falcon, C. Laroche, and S. Fauve, Phys. Rev. Lett. **98**, 094503 (2007); P. Denissenko, S. Lukaschuk, and S. Nazarenko, Phys. Rev. Lett. **99**, 014501 (2007); P. Cobelli, A. Przadka, P. Petitjeans, G. Lagubeau, V. Pagneux, and A. Maurel, Phys. Rev. Lett. **107**, 214503 (2011).
[28] L. Deike, B. Miquel, P. Gutiérrez, T. Jamin, B. Semin, M. Berhanu, E. Falcon, and F. Bonnefoy, J. Fluid Mech. **781**, 196 (2015).
[29] Q. Aubourg, A. Campagne, C. Peureux, F. Ardhuin, J. Sommeria, S. Viboud, and N. Mordant, Phys. Rev. Fluids **2**, 114802 (2017).
[30] G. Michel, B. Semin, A. Cazaubiel, F. Haudin, T. Humbert, S. Lepot, F. Bonnefoy, M. Berhanu, and E. Falcon, Phys. Rev. Fluids **3**, 054801 (2018).
[31] A. Campagne, R. Hassaini, I. Redor, J. Sommeria, T. Valran, S. Viboud, and N. Mordant, Phys. Rev. Fluids **3**, 044801 (2018).
[32] S. I. Badulin, A. N. Pushkarev, D. Resio, and V. E. Zakharov, Nonlinear Processes Geophys. **12**, 891 (2005).
[33] A. N. Pushkarev, D. Resio, and V. E. Zakharov, Physica D **184**, 29 (2003).
[34] E. Herbert, N. Mordant, and E. Falcon, Phys. Rev. Lett. **105**, 144502 (2010).
[35] M. S. Longuet-Higgins, J. Fluid Mech. **16**, 138 (1963); A. V. Fedorov, W. K. Melville, and A. Rozenberg, Phys. Fluids **10**, 1315 (1998).
[36] H. Lamb, *Hydrodynamics* (Dover, Mineola, NY, 1932).
[37] See the Supplemental Material at http://link.aps.org/supplemental/10.1103/PhysRevLett.125.134501 for movies and further data analyses.
[38] V. E. Zakharov, A. O. Korotkevich, A. N. Pushkarev, and A. I. Dyachenko, JETP Lett. **82**, 487 (2005).
[39] G. J. Komen, L. Cavaleri, M. Donelan, K. Hasselmann, S. Hasselmann, and P. A. E. M. Janssen, *Dynamics and Modelling of Ocean Waves* (Cambridge University Press, Cambridge, England, 2014).

[40] V. E. Zakharov, A. O. Korotkevich, A. N. Pushkarev, and D. Resio, Phys. Rev. Lett. **99**, 164501 (2007).
[41] A. O. Korotkevich, A. O. Prokofiev, and V. E. Zakharov, JETP Lett. **109**, 309 (2019).
[42] A. O. Korotkevich, JETP Lett. **97**, 126 (2013).
[43] S. Y. Annenkov and V. I. Shrira, Phys. Rev. Lett. **102**, 024502 (2009).
[44] A. Alexakis and L. Biferale, Phys. Rep. **767**, 1 (2018); P. Clark Di Leoni, A. Alexakis, L. Biferale, and M. Buzzicotti, arXiv:2002.08784v1.

Supplemental Material
"Saturation of the inverse cascade in surface gravity wave turbulence"

E. Falcon,[1] G. Michel,[2] G. Prabhudesai,[3] A. Cazaubiel,[1] M. Berhanu,[1] N. Mordant,[4] S. Aumaître,[5] and F. Bonnefoy[6]

[1] *Université de Paris, Univ Paris Diderot, MSC, UMR 7057 CNRS, F-75 013 Paris, France*
[2] *Sorbonne Université, IJLRA, UMR 7190 CNRS, F-75 005 Paris, France*
[3] *Ecole Normale Supérieure, LPS, UMR 8550 CNRS, F-75 205 Paris, France*
[4] *Université Grenoble Alpes, LEGI, UMR 5519 CNRS, F-38 000 Grenoble, France*
[5] *CEA-Saclay, Sphynx, DSM, URA 2464 CNRS, F-91 191 Gif-sur-Yvette, France*
[6] *Ecole Centrale de Nantes, LHEEA, UMR 6598 CNRS, F-44 321 Nantes, France*

In this Supplemental Material, we present movies (§1) and additional data analyses related to the observation of the inverse cascade in gravity wave turbulence on the surface of a fluid: Wave homogeneity (§2), wave height distribution probability (§3), and timescale separation (§4). Notations as in the aforementioned paper.

1. MOVIES

- BasinMEDcutLow.mpeg (35s - 24Mo): Large-scale wave basin seen from the shore showing the wave makers, the wall at the opposite end, the probe array, and the control room. Weak random forcing conditions.
- WeakForcingIMG_7799.mp4 (15s - 17Mo): Wave field seen from the shore. Weak random forcing conditions: Wave steepness $\epsilon = 0.063$ ($\sigma_\eta^{sat} = 0.59$ cm) and narrow spectral bandwidth (1.8 ± 0.2 Hz).
- HigherForcingIMG_7800.mp4 (15s - 16Mo): Wave field seen from the shore. Higher random forcing conditions: Wave steepness $\epsilon = 0.98$ ($\sigma_\eta^{sat} = 1.84$ cm) and narrow spectral bandwidth (1.8 ± 0.2 Hz).

2. WAVE HOMOGENEITY

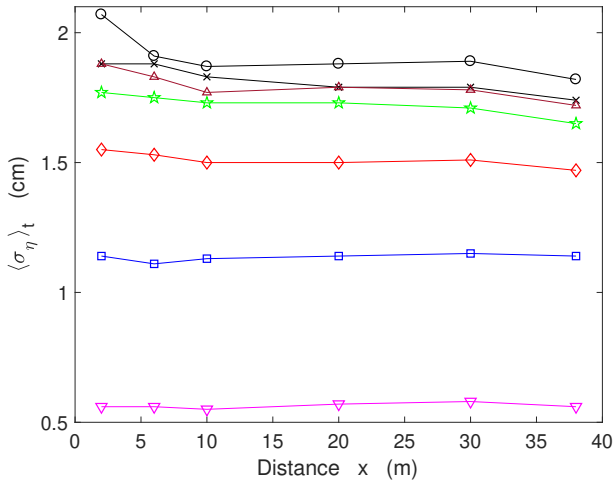

FIG. 1: Time-averaged standard deviations of wave height $\sigma_\eta(x)$ recorded at different distances x from the wave makers for different forcing amplitudes during 60 min. Good homogeneity for weak enough forcing. Same symbols as in the main paper.

3. WAVE PROBABILITY DISTRIBUTION

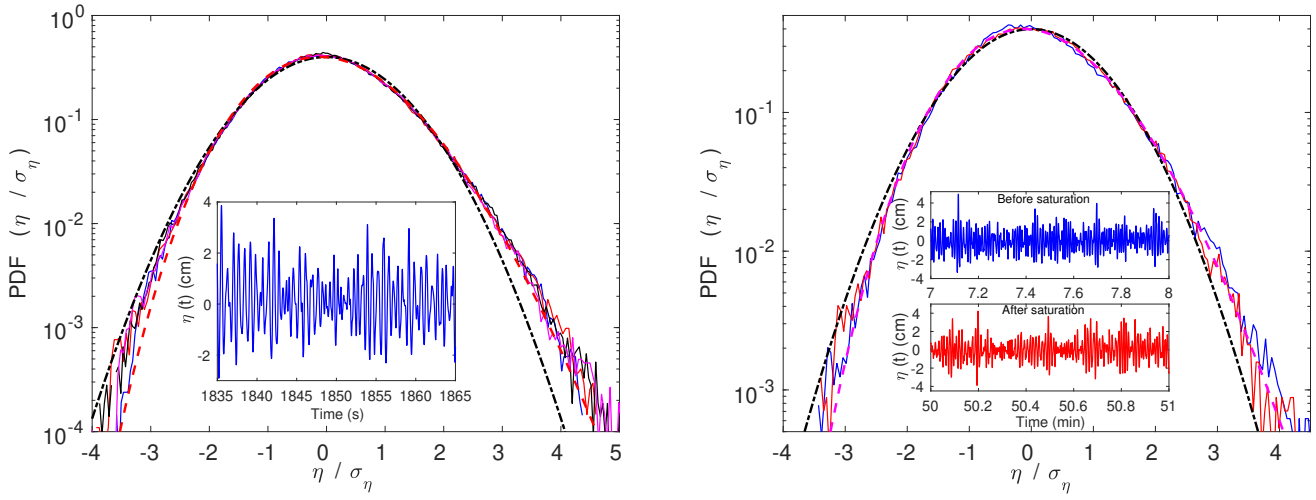

FIG. 2: **(Left)** Probability distribution functions (PDF) of normalized wave height $\eta(t)/\sigma_\eta$ recorded in the middle of the basin (x = 20 m) during 60 min and averaged on different probes [n°5 (blue), 10 (red), 11 (black), and 12 (magenta)]. $\sigma_\eta \equiv \sqrt{\langle \eta(t)^2 \rangle_t}$ = 1.14 cm. Black dash-dotted line displays a Gaussian of zero mean and unit standard deviation. Red dashed line shows a Tayfun distribution for a wave steepness of 0.08. A weak asymmetry $S = \langle \eta^3 \rangle / \langle \eta^2 \rangle^{3/2}$ = 0.23 and a weak Kurtosis $F = \langle \eta^4 \rangle / \langle \eta^2 \rangle^2$ = 3.3 are observed as expected for a weakly nonlinear wave field (Normal distribution would lead to S = 0 and F = 3). Inset displays a part of the corresponding signal $\eta(t)$ for probe n°12. **(Right)** PDF of $\eta(t)/\sigma_\eta$ computed before ($t \leq 16$ min - blue) and after ($35 < t \leq 51$ min - red) the saturation of the inverse cascade, and parts of the corresponding temporal signals $\eta(t)$ (insets). x = 20 m (probe n°12). σ_η = 1.14 cm

4. WAVE TURBULENCE TIMESCALE SEPARATION

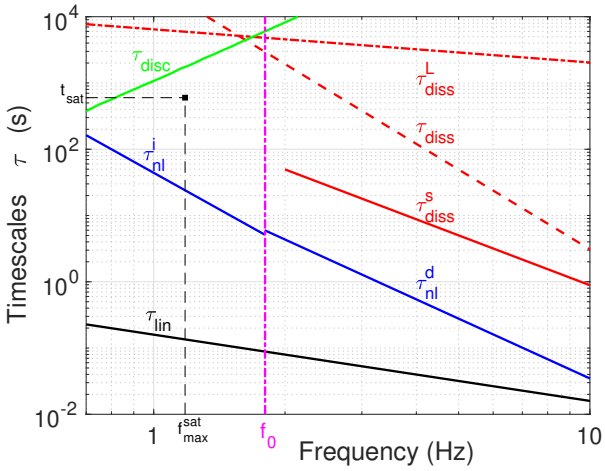

FIG. 3: Wave turbulence timescale separation. (Black solid line) Linear propagation timescale $\tau_{\rm lin} = 1/\omega$. (Blue solid lines) Nonlinear interaction timescales: $\tau^i_{nl} = c^i g^{1/6} Q^{-2/3} k(\omega)^{-11/6}$ (inverse cascade) and $\tau^d_{nl} = c^d g^{1/2} P^{-2/3} k(\omega)^{-3/2}$ (direct cascade) [4], using the values of $Q(\epsilon)$ and $P(\epsilon)$ inferred experimentally [fixed wave steepness ϵ = 0.1 (σ_η^{sat} = 1.92 cm)], the dimensionless constant value c^d = 0.03 found experimentally [28], and assuming $c^i = c^d$. (Green solid line) Discreteness time τ_{disc} computed as the number of eigenmodes found in a frequency band divided by this bandwidth, taking into account both transverse and lateral eigenmodes. No discreteness effect for $\tau_{nl} < 2\tau_{disc}$ (i.e. nonlinear spectral widening > half frequency separation between adjacent eigenmodes). Linear viscous dissipation timescales [36]: (red dashed line) viscous surface $\tau_{diss} = 1/[2\nu k(\omega)^2]$, (red solid line) surface boundary layer with an inextensible film $\tau^s_{diss} = 2\sqrt{2}/[k(\omega)\sqrt{\nu\omega}]$ negligible for $f \lesssim 2$ Hz [31], and (red dotted-dash line) lateral boundary layer $\tau^L_{diss} = 2\sqrt{2} L_x L_y / [3\sqrt{\nu\omega}(L_x + L_y)]$, L_x = 40 m, L_y = 30 m, whereas bottom boundary layer is negligible. Water kinematic viscosity $\nu = 10^{-6}$ m^2/s. f_0 is the central forcing frequency, and f^{sat}_{max} the frequency of the spectrum maximum at the saturation time t_{sat}. $\omega(k) = \sqrt{gk}$.